Journal of Thermal Analysis, Vol. 36 (1990) 1545-1577

IMPROVEMENTS IN CALORIMETRY AND THERMAL ANALYSIS APPLIED TO SHAPE-MEMORY ALLOYS

V. Torra and *H. Tachoire**

DEPARTAMENT DE FISICA UNIVERSITAT DE LES ILLES BALEARS E - 07071 PALMA DE MALLORCA
*LABORATOIRE DE THERMOCHIMIE UNIVERSITÉ DE PROVENCE F - 13331 MARSEILLE CEDEX 03, FRANCE

(Received November 24, 1989)

Calorimetric and thermal analysis set-up applied to study the martensitic transformations in shape-memory alloys is described. The information obtained are as follows: transformation temperature, enthalpy/entropy change and the dynamics of the phenomena. Hysteresis loop and the description of the macroscopic features of the transformation are given.

By means of the improved high resolution thermal analysis techniques local studies (interface movements) were performed and new phenomena, intrinsic thermoelasticity, time scales etc. were introduced.

The calorimetric and thermal analysis experimental set-up's are used to study martensitic transformation in shape-memory alloys. In some cases, it is possible to link to thermal analysis other techniques (acoustic emission, calorimetry, resistance and/or observation by microscopy leading to the simultaneous determination of several parameters [1].

In this paper, we describe the studies performed on global transformations using an unconventional scanning calorimeter designed to study solid-state transformations. Also, by improved microcalorimetric techniques, local studies of the hysteresis loop have been performed.

Besides the global studies of the hysteresis loop, local studies were performed by means of acoustic emission (AE) detection, resistance measurements and/or optical microscopy observation of the samples. For this purpose, partial cycling in accurately controlled conditions was performed on samples of Cu-Zn-Al alloy in which the growth-shrinkage of single martensite plates could be observed. The position of the interface can be

John Wiley & Sons, Limited, Chichester
Akadémiai Kiadó, Budapest

plotted *vs.* temperature thus obtaining an alternative representation of the hysteresis loop.

We present detailed analysis of the phenomenology related to a martensitic transformation in a shape-memory alloy and of the experimental resolution needed to achieve a correct description of the phenomenology. We study experimentally the effect of temperature cycles (at a constant rate in time), both at constant hydrostatic pressure and under small tensile stresses. The measurements allow one to obtain the different contributions to the energy released during a closed cycle.

Observations in the microscale domain show:

a) AE is a very sensitive tool in order to detect changes in the material;

b) AE bursts are closely released after overcoming a finite energy barrier (interface pinning);

c) thermal cycling in restricted conditions - accurately controlled temperatures and temperature rates - are necessary to obtain recoverable states.

d) time scale

e) intrinsic thermoelasticity

The global measurements give the hysteresis loop or the useful description of the macroscopic features of the transformation. In this sense, the hysteresis gives information about the frictional resistance to the interface motion, elastic energy stored/released, pinning mechanisms, coexsistence of several martensite phases, nucleation processes, time scales and others.

Martensitic transformation is shape-memory alloys [2]

A general scheme of structural phase transitions distinguishes between two main groups: diffusive and displacive transformations. Among the displacive transformations, the martensitic transformation is defined as a lattice-distortive, virtually diffusionless structural change having a dominant deviatoric component and associated shape change such that strain energy dominates the kinetics and morphology during the transformation (see Fig. 1). It is a first order phase transition occuring by nucleation and growth.

In the last few years, the interest in shape-memory alloys (SMA) has grown considerably promoting a spectacular increase in the way they can be applied. Since the shape-memory was discovered initially in nickel-titanium alloys, many studies have been made on this effect and it is now well-known to occur in numerous alloy systems both ferrous and non-ferrous. See, for example, the copper-based, the Nitinol-based or the iron-based alloys.

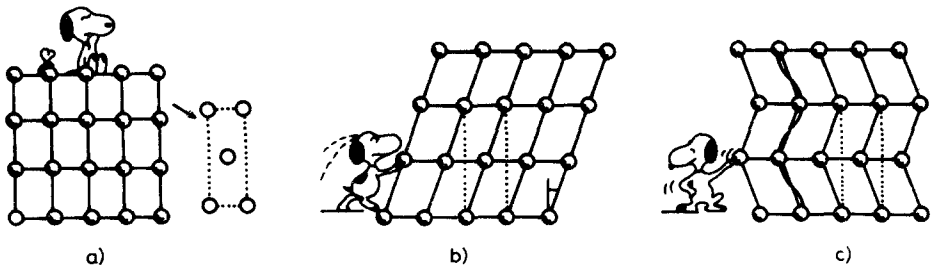

Fig. 1 a) Parent phase; b) Transformation by uniform shear; c) Transformation by shuffling (from F.E. FUJITA, ICOMAT 82, p. 10-17)

There is a definite connection between the atom positions in the parent and martensitic phases; the composition remains fixed and the material can be treated as a single component system. The two phases (parent and martensite) coexist during the transformation. This structural transition gives rise to a macroscopic shape change. The main transformation mechanism is a homogeneous shear. Accordingly, an externally applied stress field provides the shear stress to couple with the transformational shear strain. The transformation can be either thermally or stress-induced.

The strain energy accompanying the martensitic transformation is accomodated in matrix and product phase in one of two ways: plastically, by mechanism like slip and twinning (as in steels and in most of the iron-based alloys) or elastically as in noble metal-based alloys. In the last case, the energy associated with the martensitic shape and volume changes is elastically stored in the material during the forward transformation and reverted during the reverse transformation. The process takes place in quasi-equilibrium condition which gives the name thermoelastic to these transformation.

Experiments show indeed that a thermoelastic martensitic plate grows or shrinks continuously as temperature is lowered or increased, in an equilibrium between chemical and non-chemical (mainly elastic and frictional) forces. The elastic forces tend to hinder the forward transformation and favour the reverse one, while the frictional forces will always oppose the transformation. An energy balance equation takes into account the internal energy change due to the transformational entropy change, the internal storage of elastic energies, the coupling with external stress fields and the dissipative energy contributions.

Recently, new ideas appear in this domain: the intrinsic thermoelasticity in the stress free measurements (a single interface in a single variant transformation).

Some phase transformations which are concomitant with the martensite formation may complicate the picture. See for example, the order-disorder transformation or the formation of surface martensite in copper-based alloys. Also, under certain conditions, the time, thermal or load cycles can bring about significant changes in the transformation temperature, shape reversibility or work performing capacity. These are otherwise known as stabilization of the martensite or the beta phase, ageing and degradation. These phenomena are related to the presence of different kinds of defects (vacancies, dislocations, precipitates) in the martensitic lattice, the state of order and the generally metastable state of the lattice. Also, some martensites can change into other martensitic configurations when load is applied. These martensite - martensite transformations are also temperature dependent and recoverable under appropriate conditions. Defects, such as dislocations in the samples, are introduced to a large extent by thermal and mechanical cycling. The way they affect temperatures, enthalpy changes and hysteresis of transformation is more important.

It is fundamentally interesting to distinguish from a theoretical point of view between equilibrium properties and kinetic concepts. The former refers to the characterization of the phase transformation associated with equilibrium thermodynamics, whereas the latter refers to the description of the actual process of the phase transformation and its evolution in time from an initial to a final phase. First order phase transitions generally exhibit the possibility of hysteresis cycles and associated metastable states. The decay of such metastable states to equilibrium is a kinetic process named nucleation triggered by fluctuations and characterized by an energy barrier which determines lifetime of the state. The growth of domains of the new phase formed during the transformation may occur via different mechanisms.

Also in stress free transformations, pinning effect induces metastability and burst-like interface movement or new nucleation processes.

Heat-conduction calorimetry [3-5]

Heat-conduction-calorimetry is now a well established technique in widespread use and a lot of instruments are commercialy avaliable. The differential mounting of two identical elements ensures a great stability in time. Equipped with semiconductor thermocouples, they possess a high sensitivity

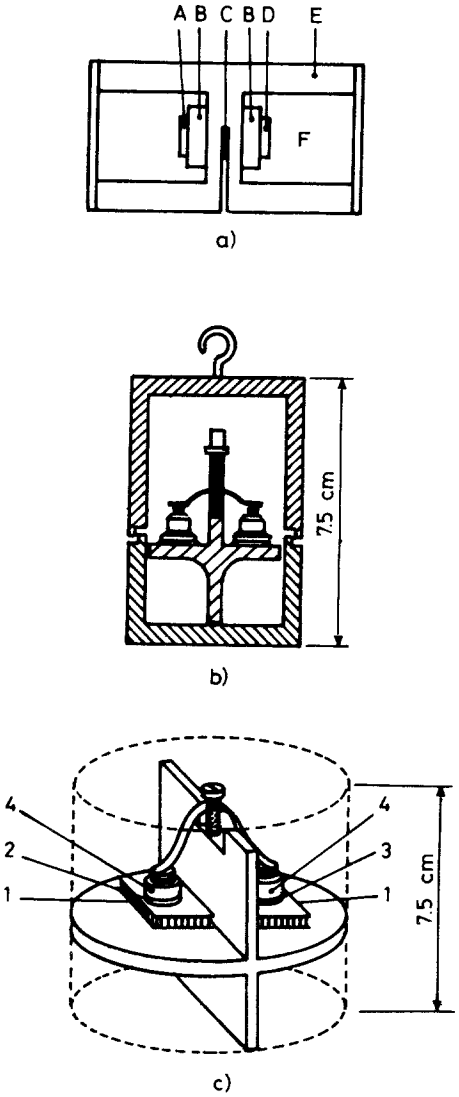

Fig. 2 a) Schematic drawing of an actual calorimeter A) reference sample; B) thermobatteries (Melcor FC 0.6-66-05L); C) temperature sensor (Pt-100); D) sample, E) calorimetric block (isothermal or low temperature rate); F) additional available working space
b) Actual differential-heat-conduction-scanning calorimeter
c) Differents parts; 1) Melcor thermobatteries; 2) sample; 3)reference material; 4) acoustic detector (piezoelectric)

(about 400 mV/W at room temperature) and are easy to operate in the range from 200 to 370K (Figs 2a, b, c).

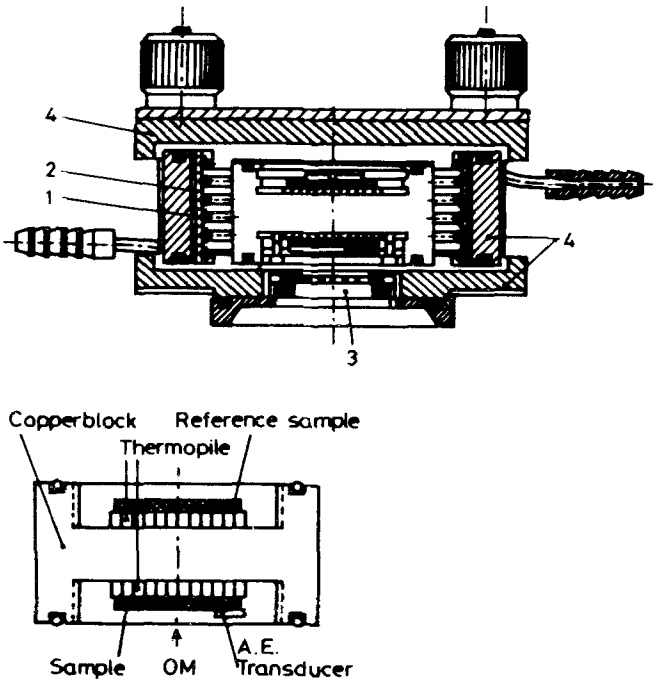

Fig. 3 Heat-conduction-calorimeter with acoustic emission detection and optical microscopy. 1) cooling coil; 2) heating resistance (Thermocoax); 3) observation window; 4) Brass box; (OM) Optical microscopy

The response of these instruments contains the dynamics of the energy production of the studied phenomena distorted by the inertia of the apparatus. The techniques of acquisition and processing of data allow compensation of this inertia. In certain cases, it is possible to link to the calorimeter other techniques of measurement and/or observation (see, for example, acoustic emission, resistivity or optical microscopy) leading to the simultaneous determination of several parameters and hence to a better understanding of the phenomena (see Figs 2, 3 and 4). Also, new systems are constructed with sophisticated and computerized temperature rate control and programming (Figs 5 and 6).

In their design, the calorimeters described above present a geometry which is quite similar in many aspects to the commercial DSC and even DTA

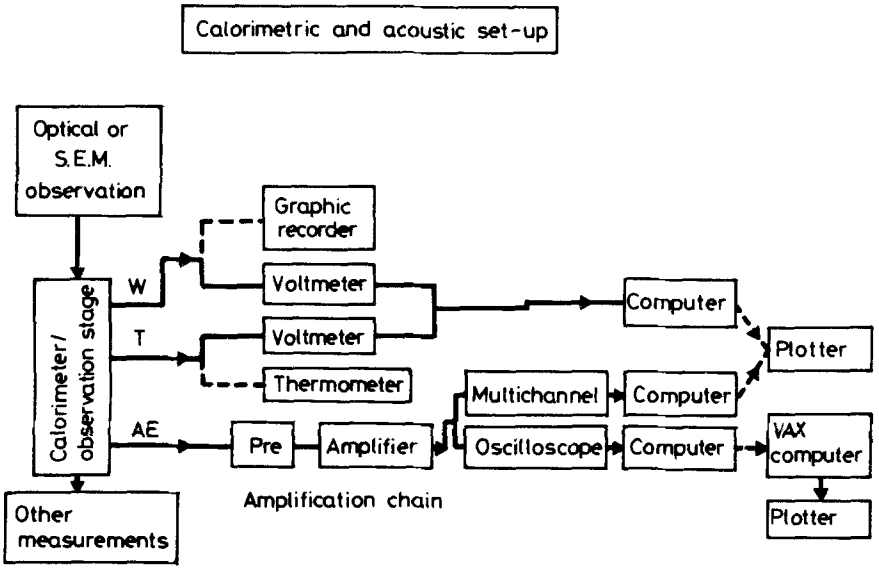

Fig. 4 Experimental set-up. Equipment designed for the simultaneous measurement of thermosonimetry and calorimetry

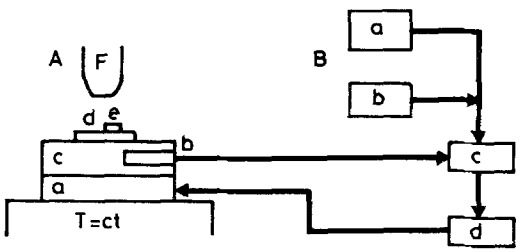

Fig. 5 New improvements in thermal analysis. A) experimental system, a) Peltier effect; b) temperature sensor Pt-100; c) copper; d) sample; e) piezoelectric transducer; F) microscope
B) Temperature control and programming, a) transfer function; b) choice of the $T(t)$; c) calculus of the $I(t)$; d) dynamic control

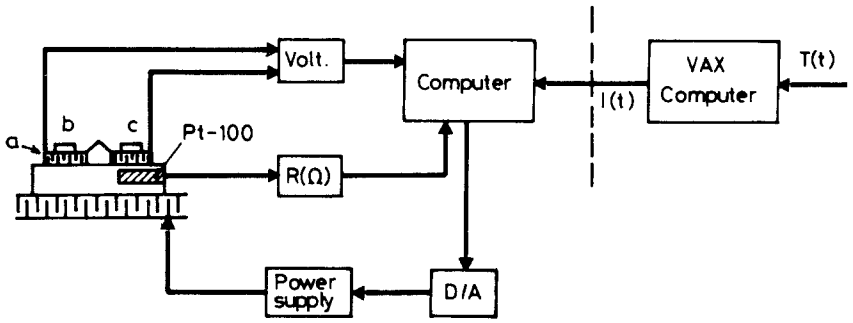

Fig. 6 Unconventional DSC with temperature control and program - System derived of the set-up outlined in Fig. 5 a) thermobatteries in differential form; b) sample; c) reference material

but they do not utilize automatic compensation. The commercial devices have been extensively studied by different groups, with the aim of better understanding the meaning of the calorimetric output which seems to be highly influenced by the temperature programming. In fact, the problems of commercial DSC are mainly caused by the high temperature-scanning rates at which it normally operate. Our calorimeters operates at much lower rates of temperature programming (near 0.3 deg/min in the spontaneous heating/cooling). Additionally, neither melting processes nor important changes in specific heat are involved in a martensitic transformation.

The calorimetric set-up and its performances [3-5]

The device is formed by a calorimetric block (built in copper to improve its thermal conductivity) in which two MELCOR thermobatteries are differentially assembled. Both samples, the reference sample and the material under test, are placed on the top flat side of the thermobatteries. The top surface of the samples is left free and can be used to place other tranducers in order to perform coupled measurements. The differential output signal is converted to the digital signal by a voltmeter (resolution 100 nV) and send to the memory of a microcomputer which finally stores the information on magnetic support for further analysis. Simultaneously, the temperature of the calorimetric block is measured by means of platinum resistance Pt-100 and also stored by the microcomputer.

Under normal working conditions, noise in the base-line centers around ± 200 nV. During the martensitic transformation of a copper-based alloy, samples with a mass of 0.5 g produce signals around 1 mV.

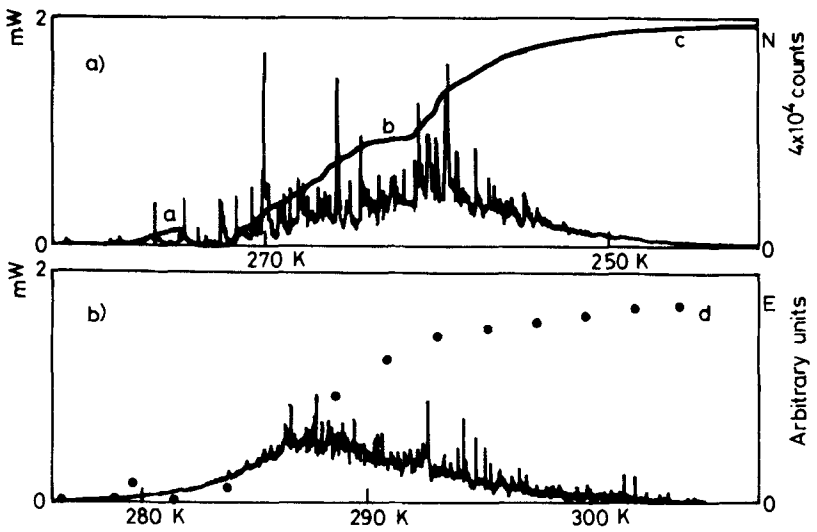

Fig. 7 a)Thermal curve from parent phase to martensite in 81.2 Cu, 11.8 Al, 6.8 Mn, 0.2 Fe (wt %); a, b, c) accumulated number of counts shown as a function of temperature b) Reverse transformation (martensite to parent phase); dots) accumulated acoustic energy in arbitrary units

Often, the signal-to-noise ratio has a value of 5 000 (for $\beta - \beta'$ transformations) and, on certain occasions, it can reach 10 000 ($\beta - \gamma'$ transformations). After studying the impulse response of several similar devices, we give for the main time constant an approximate value of 10 s for mass near 0.5 g and in thermal equilibrium. When this is taken into account, very fast thermal dissipations (burst-like transformations) giving signals above one μV are clearly visible on the thermogram. In the first approximation, impulse signals close to 10 μVs can be resolved. As the sensitivity of the detectors near room temperature is approximately 400 mV/W, the final energy resolution of the device is about 25 μJ. The martensitic transformation in Cu-Zn-Al alloys typically releases or absorbs 6 J/g and, consequently, the calorimeter should be able, in principle, to detect instantaneous transforming portions of mass near 4 μg.

Under the assumption that scanning the temperature at low rates does not modify the dynamic properties of the calorimeter, the thermal processes taking place in the material are detected with high accuracy in time and temperature. For example, on the thermogram, the capability of distinguishing between two sudden and elementary transformations occurring with time difference near the value of the main time-constant, i.e. with a difference in temperature of only 0.05 K is possible. An inverse filtering of the thermogram, using two or three time-constants, increases the temporal resolu-

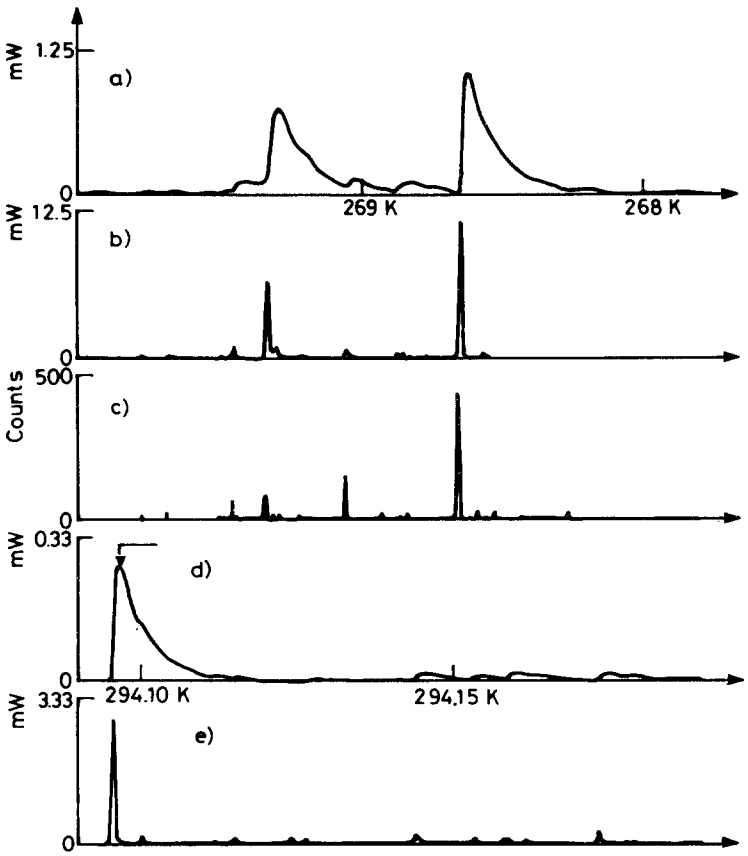

Fig. 8 Kinetic study of a limited interval in the $\beta \rightarrow m$. a) thermal curve; b) thermogenesis by inverse filtering; c) acoustic emission (counts rate); d) local study of the $m -> \beta$ transformation; e) thermogenesis, the first pulse is near 2s width

tion by two orders of magnitude. This, in principle, gives resolution able to separate signals to 0.001 K or less.

If the temperature scanning is carried at lower or much lower rates, the resolution in temperature increases correspondingly. This will probably be inadequate when studying the transformation as a whole, as it extends often through an interval of 20 or 30 K but always very interesting to study local phenomena (see Figs 7,8 and 9). In the present state of the art, in fact, the required computer calculations are rarely done and this high resolution is never achieved. This is mainly because the high resolution demands data acquisition at sampling rates around 0.05 s (near 20 Hz) and the storage of approximately 100 000 calorimetric data per transformation for further analysis.

Also, at very low temperature rates unctrolled procceses appear (see, for instance, stabilization).

Calorimetric models and energy measurements [5-7]

The models which have been commonly used to describe the different devices are based on heat-transfer equations written for localized constants:

$$W_i = C_i \left(\mathrm{d}T_i / \mathrm{d}t \right) + \sum_{k \neq i}^{N} P_{ik} \left(T_i - T_k \right) + P_i \left(T_i - T_o \right)$$
$$i = 1, 2, ..., N$$

The form of the heat-balance equations is the starting point for determining the transfer function or transmittance $h(t)$ (response to one Dirac pulse) which characterizes the dynamic (and static) properties of a given calorimeter. By applying the Laplace transform to the previous equation, the $h(t)$ can be written in the form

$$h(t) = \sum_{i=1}^{N} a_i \exp \left(-t / \tau_i \right)$$

From $h(t)$ and the heat power $W(t)$, simulated thermograms are easily obtained via the convolution integral. Obviously, if T_o is not a constant, only numeric approaches are possible (see, for instance, solving the differential system equation's via the Runge-Kunta method).

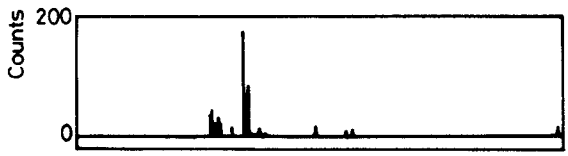

Fig. 9 Acoustic emission. Corresponds to the first 10 s of the high calorimetric signal pulse (Fig. 8d) and shows the internal bursts structure

The Tian equation represents the simplest possible model of localized constants in which only one element is considered. For a time-invariant system with C as the heat capacity, P as the thermal coupling to the thermostat and $W(t)$ as the thermal power released in the calorimetric cell as a function of time, and if a constant temperature is assumed in the thermostat (T_o = 0), the Tian equation reads

$$W(t) = C\,(\mathrm{d}T/\mathrm{d}t) + PT$$

If the reference temperature is programmed as a function of time, the system is now a time-varying one.

When the temperature changes, there will be at least a progressive contribution due to radiation between the heat capacity C of the calorimetric vessel and the surroundings. As the usual temperature scanning rates are rather low, the temperature differences will be very small. In this situation, for large intervals of the temperature $T_o(t)$ and as a first approximation, we can consider the thermal coupling to be caused by a double contribution

$$P = P_o + P_1 \tilde{T}^3$$

where $\tilde{T}$ is an average temperature between the temperatures of the cell and the surroundings. Linking the electric output signal with the temperature differences via the Seebeck effect gives

$$s(t) = A\tilde{T}\,(T_1 - T_o)$$

Considering that the actual calorimeter is a differential one, we have to include a second passive element in the model, with no direct thermal couplings to the first element (see Fig. 10a) and we get:

$$W(t) = (1/A\tilde{T})\,(C\,(\mathrm{d}s^*(t)/\mathrm{d}t) + (P_o + P_1\tilde{T}^3 - ((C/\tilde{T})\mathrm{d}\tilde{T}/\mathrm{d}t)\,s^*(t))$$

where $s^*(t) = s(t) - s_{ref}(t)$ and $s_{ref}(t)$ the signal given by the reference thermobattery. Figure 10 b shows the agreement between the sensitivity at constant temperature $S(\tilde{T})$ and the experimental results. The qualitative agreement is to be emphasized in light of the crude description given by the model and the approximations that we have been using.

To obtain the total energy involved in a transformation, we integrate the thermal power W(t) from the time t_1 at which the process begins until the time t_2 at which it ends

It is clear that the utilization of the static sensitivity as obtained from the isothermal test measurements gives the correct result but only if there are not important changes in the heat capacity C during the process.

Signal processing [5, 7]

The deconvolution techniques are based on the fact that calorimetric devices may be considered as linear systems. It is commonly accepted that there exists a linear relationship between "cause" and "effect" amplitudes. This functional relationship does not change under a given set of experimental conditions. When these conditions change to any marked degree, though a linear relationship still exists,

its functional expression will be obviously different.

The linearity of the instrument must be tested by analysing its behaviour under addition of different input signals and multiplication a given input signal times an arbitrary scalar factor. Here, we can use either power steps (Heaviside functions) or impulses (Dirac pulses).

The calorimetric system (invariant system or constant temperature) is now considered as a black box. The first step is to identify the system, in other words, to obtain its transfer function. This identification must be performed under conditions resembling as closely as possible those of the thermogenesis to be reproduced. In view of the fact that the geometrical and thermal properties of the calorimetric device and the location of the heat source remain unchanged (both during the identification of the system and during the process under study), this is difficult to achieve in our case.

The functional relation between the input e(t) (which is proportional to the thermogenesis or heat power) and the output s(t) (thermogram) may be written

$$s(t) = M(e(t))$$

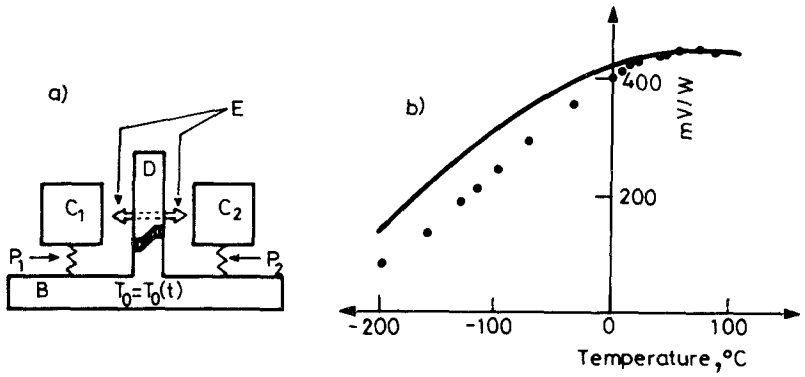

Fig. 10 (a) Calorimetric model: B and D) calorimetric block, C_1 and C_2 heat capacities; P_1 and P_2 thermal coupling between heat capacities and calorimetric block E) direct thermal coupling between the samples; (b) Sensitivity (mV/W) *vs.* temperature dots) experimental values; line) Sensitivity with coupling accounting for radiation

In the Laplace space, the linear relation between the input and output may be written now

$$S(p) = H(p)\,E(p)$$

The transfer function $H(p)$ is the transform of the impulse response $h(t)$. From calorimetric models, via localized constants, the $h(t)$ reads

$$h(t) = \sum_{i=1}^{N} a_i \exp(-t/\tau_i)$$

Namely,

$$H(p) = S\left(\prod_{i=1}^{M}(\tau_j^* p + 1) \Big/ \prod_{i=1}^{N}(\tau_i p + 1)\right) \quad (S = \text{sensitivity})$$

The $-1/\tau_i$ are the poles and $-1/\tau_j^*$ the zeros of the transfer function. We usually need a few terms in the products because the sequence of time-constants $\tau_1, \tau_2, \tau_3, \ldots$ decreases very quickly.

The calorimetric response is speeded up to a remarkable extent by using the iterative inverse filtering. Applying to the response $s(t)$ the operation

defined by the expression

$$s_1(t) = s(t) + \tau_1 \, ds(t)/dt$$

we obtain a signal in which the first time-constant no longer has any effect. On the other hand, if we apply to s(t) the operation defined by the relation

$$s(t) = s_1^*(t) + \tau_1 \, ds_1^*(t)/dt$$

we obtain a signal $s_1^*(t)$ in which the effect of the first zero of the transfer function is lost.

The signal processing is a more generalized technique. It is applicable to the temperature control and programming. The temperature control is performed with a feed-back loop operating (Pt-100) resistance (the "thermogram $s(t)$") and the intensity used in Peltier effect (The "heat power $W(t)$").

Calorimetry of the copper-based alloys [3, 5]

Martensitic transformation are associated with a hysteresis in transformation temperature. Hysteresis appears when the reverse transformation takes place at higher temperatures than the direct one. It is well-known that hysteresis cycle provides a description of macroscopic features of martensitic transformations in shape-memory alloys. In the literature, the width of hysteresis loop provides information about the frictional resistance to the interfaces motion; the inclination of transformation curves is associated to elastic energies and mixed forms relied at new phases.

Furthermore, the area enclosed in a "reversible" hysteresis loop drawn in the entropic diagram (temperature-entropy coordinates) obviously represents the heat released or the work lost in the cyclic process. Changes in the hysteresis loop by cycling are relied to irreversible process in the material inducing changes in the transformation path.

The study by thermal analysis (unconventional DSC and acoustic emission AE or thermosonimetry) shows the effects of thermomechanical treatments on the global hysteresis cycle for a Cu-Zn-Al single crystal. Experimental measurements proof the relevant role of the defects on the transformation. The effect of thermal cycling, defects concentration after

thermal treatment, annealing and different cutting orientation in mechanically cycled materials has been studied.

To study global transformation $\beta \leftrightarrow m$, an unconventional differential scanning calorimeter (DSC) is used able to work in the range 80 - 400 K (see Fig. 2). With usual temperature scanning rates of near 0.3 deg/min, the temperature resolution (without signal processing) is about 0.005 K. Additionally, this device permits to perform simultaneous coupled measurements of acoustic emission. By its design, it is specially appropriate to describe transformation dynamics.

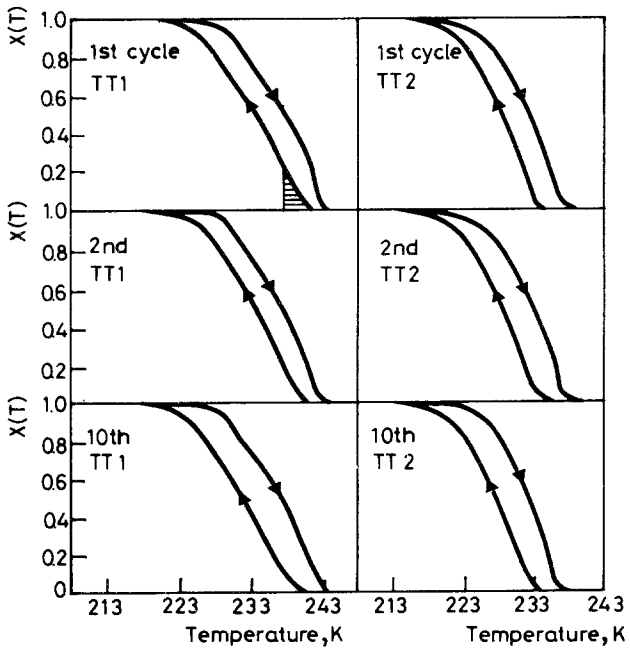

Fig. 11 Hysteresis loops in relative transformed fraction ($x(T)=1$ implies martensite); left) Heat treatment TT1, cycles 1, 2 and 10); dashed zone is connected with the initial growth process; right) Heat treatment TT2, cycles 1, 2 and 10

DSC studies have been made with single crystal alloy Cu 68.1 - Zn 16.2 - Al 15.7 at.% with an electron to atom ratio e/a = 1.48 and nominal Ms near 240 K. Several samples of 6 mm diameter and about 1 mm thickness were studied. Study of the annealing effects was done with several samples of the polycrystal Cu-Al-Ni (Cu 69.2, Al 27.6, Ni 3.2 at. %). Also, samples of the alloy with Ms over 273 K (Cu 68.5, Zn 14.9, Al 16.2 at %) were used in local

studies. Hysteresis cycle was obtained from the several extensive quantities versus temperature representation for the forward and reverse transformation. Quantities used are, for instance, the enthalpy, the "entropy" obtained from $\int \delta Q / T$ and, in the local studies, the interphase position.

Thermal treatments and cycling [3]

In this case, samples were maintained for 10 min at 1123 K and either cooled in air at room temperature (TT1) or quenched in water at 273 K (TT2). Thermal cycling between 200 and 300 K at a mean temperature scanning rate (dT/dt) near 0.3 deg/min was initiated 24 h after treatment to stabilize the spontaneous ordering processes.

Comparative study of thermal energy released during the first cycle of transformation for heat treatments TT1 (air quenching) and TT2 (water quenching) in several samples (Fig. 11 left and right) establishes that, after the TT1, the transformation starts with a sudden energetic dissipation in a reduced temperature domain. After that initial part, the transformation gradually progresses.

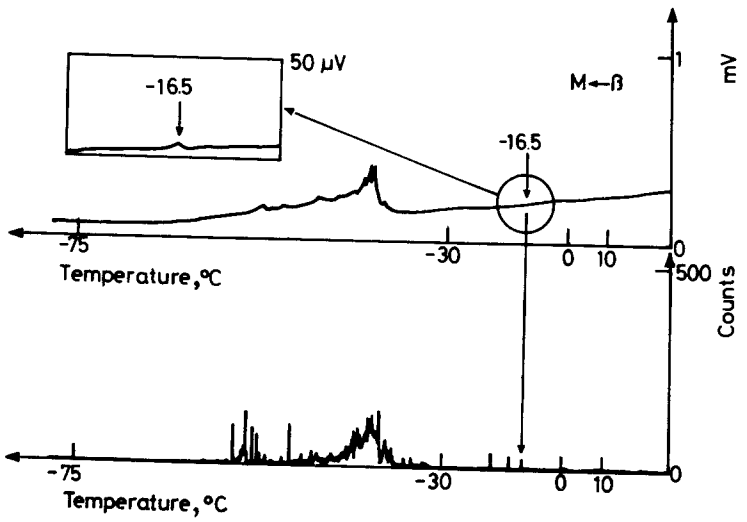

Fig. 12 Calorimetric thermogram (top) and acoustic emission (bottom); Acoustic emission bursts are correlated with calorimetric micropulses; thermogram in the window x 20

On the other hand, after thermal treatment TT2, transformation starts with small independent calorimetric pulses (corresponding to elementary transformation of near 30 μg of material and energy about 180 μJ) at

temperatures higher than Ms (TT1) (20 K or more). These microtransformations are unobservables at the usual working scale (standard DSC resolution near 1 mg). Simultaneous AE recording shows correlated burst (see Fig. 12). After that, the transformation starts with an increasing mean growing in all transformation temperature domain. The temperature extension and hysteresis width of $\beta \rightarrow M$ and $M \rightarrow \beta$ transformation is larger for TT2 than for TT1. Optical observations of the transformation agree with the obtained thermograms. TT1 starts with a quick growth of big martensite plates. After quenching (TT2), few isolated microplates are observed. TT2 starts with a lot of small plates which need a continuous increasing of thermodynamic driving force (temperature decreasing) relied to mechanical interaction between plates, to grow.

When changing the surface state of one sample doing different degrees of surface polishing (mechanical and chemical polishing) after thermal treatment TT1, the difference Ms-Af increases, consequently, the fraction of material corresponding to the initial part of the transformation (only 2 K) also increases as can be seen in Fig. 13 (a and b) (see also "Nucleation and growth").

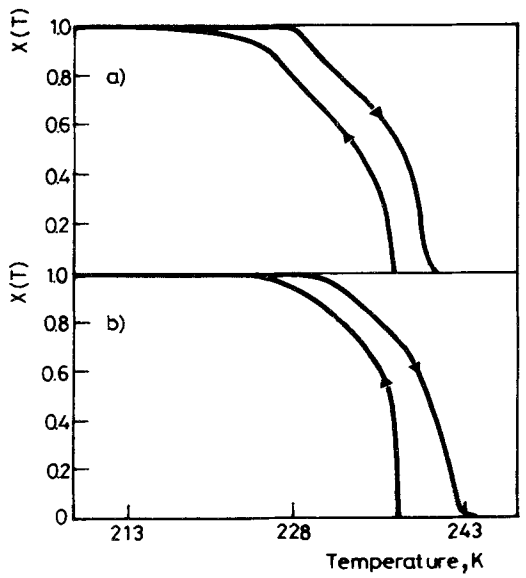

Fig. 13 Hysteresis loops in relative transformed fraction *vs.* temperature a) Mechanically polished before TT1; b) Electrolytically polished before TT1

If the tenth cycle is observed, an increase in the hysteresis width with respect to the previous ones can be seen for the TT1 case, while no perceptible change is observed for the TT2 one. The increase in the defect concentration (in TT1) leads an enhancement of the frictional work as it has been pointed out by the increasing of the hysteresis width. This effect is mainly due to the shift of the forward transformation curve, indicating that different frictional mechanisms hold for both the forward and reverse transformations.

Annealing and thermomechanical treatments [3]

After quenching to room temperature samples of Cu-Al-Ni, two phases, namely the orthorombic β' and the hexagonal γ', were observed to coexist in the martensitic state, instead of the expected γ'. This results in a mixed hysteresis loop as can be seen in Fig. 14. The appearence of the β' martensite is closely related to the high internal stresses built up in the sample as a consequence of the γ' burst growth. The β' progressively dissappears after annealing for variable times at 473 or 573 K which is reflected in the corresponding hysteresis loops. Annealing acts in two ways: on the one hand, by ordering processes, it increases the transformation temperatures. On the other hand, it decreases the quenched-in defects concentration making the γ' growth smoother. As a consequence, both the slope increases and decreases the hysteresis width.

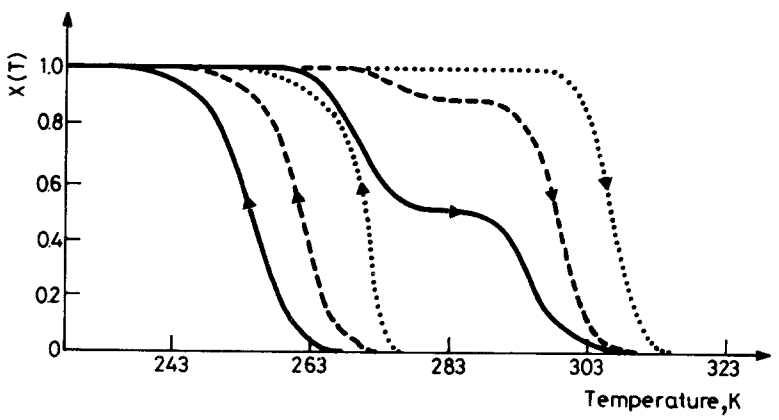

Fig. 14 Hysteresis loops in relative transformed fraction *vs.* temperature obtained after different annealing times (t) at 573 K; continuous line) $t=0$ s; dashed line) $t=22$ s; dotted line) $t=55$ s

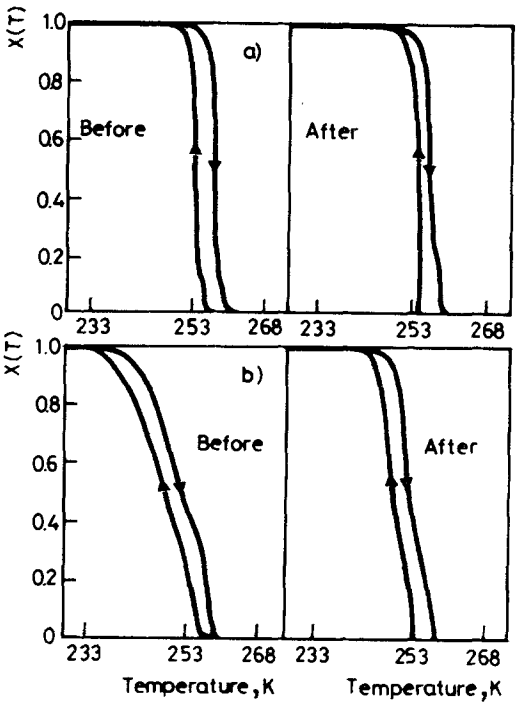

Fig. 15 Hysteresis cycles obtained before and after the heat treatment to remove the training effect for samples cut a) parallel and b) non parallel to the habit plane

Samples of Cu-Zn-Al were submitted to a training process (by means of repetitive mechanical cycling) which leads to the preferential formation of one or few martensite variants. After that, they were cut in different orientations relative to the habit plane. Calorimetric hysteresis cycles are shown in Fig. 15. Our results indicate how the surface orientation plays a very important role in the transformation dynamics. After untraining heat treatments (6 hours at 1 123 K), the hysteresis cycle changes. Width diminishes and slope decreases for the samples cut parallel to the habit plane. However, microscope observations pointed out that mainly the same variants were formed before and after the "untraining" thermal treatment.

Nucleation and growth [3]

Nucleation of the martensite phase inside the β-matrix have been a subject of particular interest recently. From a theoretical point of view, it is assumed that defects play a very important role in assisting martensitic

nucleation. However, from an experimental point of view, there is a definitive need of quantitative information, especially in the case of Cu-Zn-Al alloys. It has been proved recently that, by means of a suitable thermal treatment, it is possible to vary the Ms temperature while Mf, As and Af remain unchanged. This allows one to study the nucleation process separately and its influence on the transformation hysteresis.

The analysis of the hysteresis loops obtained by means of the calorimetric technique for thermally - induced transformation cycles in a Cu-Zn-Al allows us to provide quantitative information about the critical driving force for nucleation. In our criteria, "nucleation" is identified with the initial observable growth. Optical microscopy observations of the sample, together with the calorimetric study, give new insights about the kind and location of the most favourable defects for the martensitic nucleation.

Single crystal samples with nominal composition 15.93 Al, 16.13 Zn, balance Cu (at %) have been used. Previously to the thermal treatment (TT1 type), the samples were mechanically and electrolytically polished. Auxiliary observations were performed in an optical microscope, Olympus BH-2, with maximum amplification 700.

Figure 16 (left) shows the calorimetric response corresponding to the forward transformation in the lst and 2nd cycles. Figure 16 (center) shows, in its turn, the hysteresis loops corresponding to the 1st and 2nd cycles and to the 1st and 10th cycles. In the first cycle, the initial growth stage takes place with an explosive thermal power dissipation which can involve almost 50% of the total energy change in a very narrow temperature interval. After the tenth cycle, the sample was electrolytically polished again and the subsequent eleventh thermal cycle was recorded (see Fig. 16 right). It was observed that Ms(11) lies close to Ms(10) or Ms(2). On the other hand, the hysteresis width, measured at 50% of the total heat released, increases from the 2nd to the 10th cycle and is maintained or even increases in the 11th one.

In most of the studied cases, the acoustic emission released during the transformation was simultaneously monitored by means of an amplification set-up and a multichannel analyzer (Canberra 35). It was observed that no acoustic activity is recorded until the Ms temperature is reached.

The first steps of the transformation were observed by means of optical microscopy with polarized light for several consecutive cycles. The sudden appearance of the first martensite plates in the 1st cycle prevents our recording it. Conversely, the disappearance of the last plates, which in all

the observed cases were the first that were formed, occurs more slowly, so allowing to localize the zone in which the martensite nucleates.

In these conditions, it could be observed that the nucleation sites are different in the first and second cycles, since the transformation started from different zones of the sample. From the second cycle on, the transformation starts from the same zone of the sample. In all the observed samples and cycles, the nucleation occurs in the edges of the sample, without any clear relationship with the low-angle domain borders.

After the first cycle was completed, some traces rest in the sample surface corresponding to residual deformation. Even small amounts of retained martensite, usually in those zones where different martensite variants interacted during the forward transformation, could be observed. This retained martensite does not completely disappears during the reverse transformation but heating up to 20 K above the Af temperature. In the next transformation cycle, some growth of this martensite could be observed but the transformation does not start from it but it begins in another nucleation sites.

The undercooling needed to start the transformation in the first cycle produces a fast growth of the first martensite plate of non/thermoelastic. After this, the interaction between plates of different variants is evidenced and the rest of the transformation occurs under thermoelastic equilibrium, as the whole reverse transformation do. In the second cycle, the thermoelastic character is evidenced since the beginning of the transformation, and from point A onwards, the curves are coincident for both the 1st and 2nd cycles. This means that the defects created (or activated) by the first cycle do not influence the elastic terms of the transformation from a global point of view.

The increase in the hysteresis width from the 2nd to the 10th cycles is to be attributed to the enhancement of the frictional work due to the creation of defects that takes place by cycling. This defects, however, do not play any role in assisting nucleation, as evidenced by the fact that Ms is not modified from the 2nd cycle on.

New trends in thermal analysis [5]

The local study of the transformation in restricted temperature domain has been done with an optical microscope Olympus BH-2 (maximum amplification x 700) and by AE detection with standard techniques (ring-down type and / or burst-counting). The experimental set-up (see Fig. 5) is

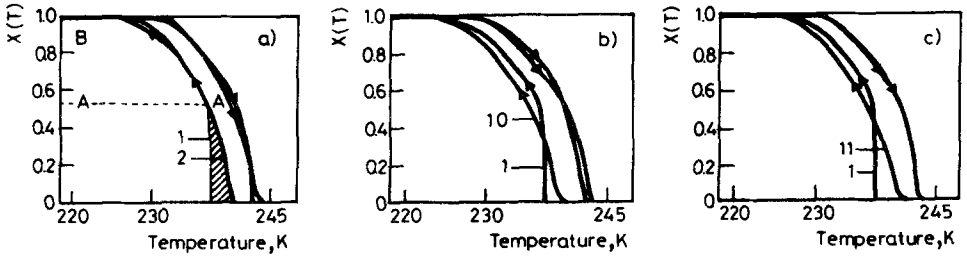

Fig. 16 Hysteresis loops *vs.* temperature; a) 1st and 2nd cycles, lined area corresponds to the excess of area (driving force necessary at initial step of growth) enclosed by the first cycle; b) Loops for the 1st and 10th cycles; c) Loops for the 1st and 11th cycles (after new electrolytical polishing)

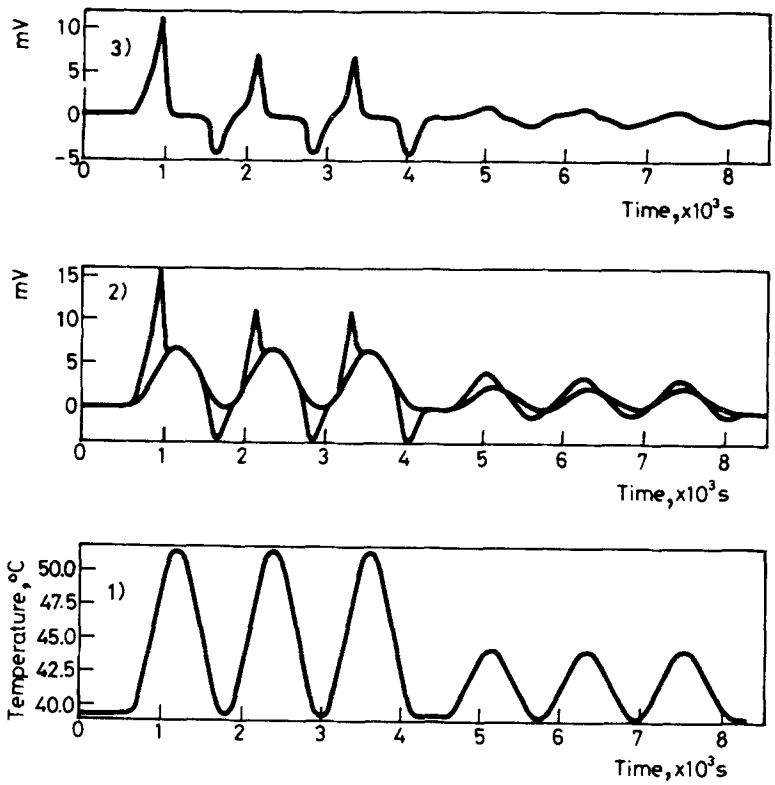

Fig. 17 Time representation; 1) Temperature vs. time; 2) Base-line and thermogram; 3) Thermogram without base-line effects

temperature controlled by computer (resolution better 0.005 K). The microscopic observations are stored in videomagnetic tape for further study.

Also, the experimental set-up is expanded to obtain the calorimetric thermograms (see Fig. 6) with more general temperature rate and evolution of the $T(t)$. For this system, the noise in the base-line is near 1 μV. In the Fig. 17, temperature programming, thermogram and base-line are presented.

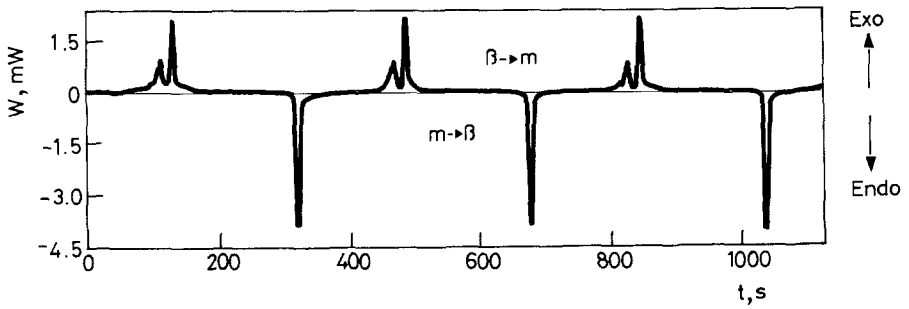

Fig. 18 Thermal curves (in mW) for several cycles of the elementary - single interface and stress free - processes. Temperature span 0.4 K. Energy for the β to martensite transformation (near - 28 mJ) equals the energy of the reverse transformation

For this experimental set-up (standard energetic measurements), the reproducibility in the enthalpy changes appears in the following table (differences are related to the base-line and metastability effects):

Cycle	ΔH ($\beta \rightarrow m$), J	ΔH ($\beta \rightarrow m$), J
2	-1.38	1.58
3	-1.37	1.52
4	-1.38	1.51
5	-1.37	1.53
6	-1.37	1.51
7	-1.39	1.54

Simultaneous optical observations and AE activity detection with a high resolution temperature control determine, via the AE, the temperature resolution necessary to obtain true thermoelastic (recoverable) processes. Also, the hysteresis loop for single plate growing/shrinking in a single crystal sample have an intrinsic character showing an intrinsic thermoelasticity.

The "transformation *vs.* temperature rate" dx/dT (x = martensite per cent) is a function of dislocation concentration. The hysteresis width is time

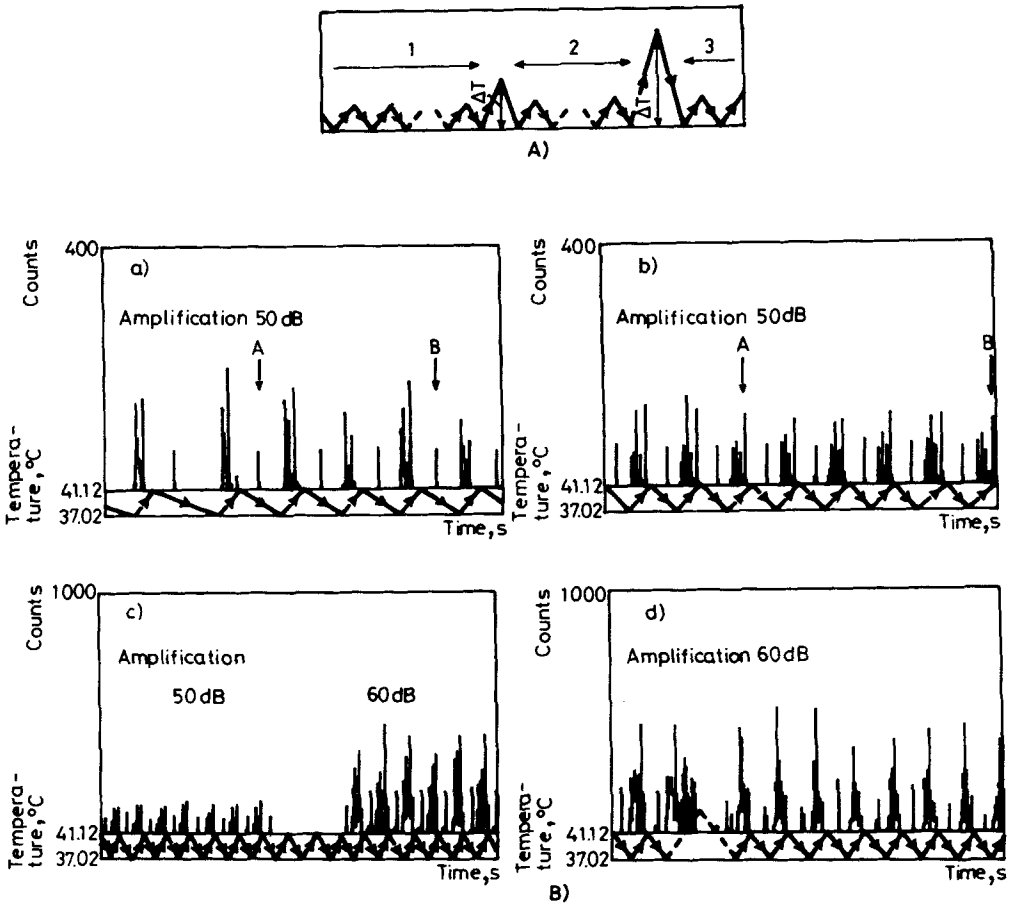

Fig. 19 (A) Thermal cycling to study reversibility and stochasticity via the AE in SMA: zone 1, zone 2, zone 3. Acoustic emission (burst counts) and temperature *vs.* time; arrows indicate equal AE bursts; a) zone 1; b) zone 2; c) zone 2 with two acoustic amplification; d) zone 3, instead of only one cooling pulse, two different pulses appear

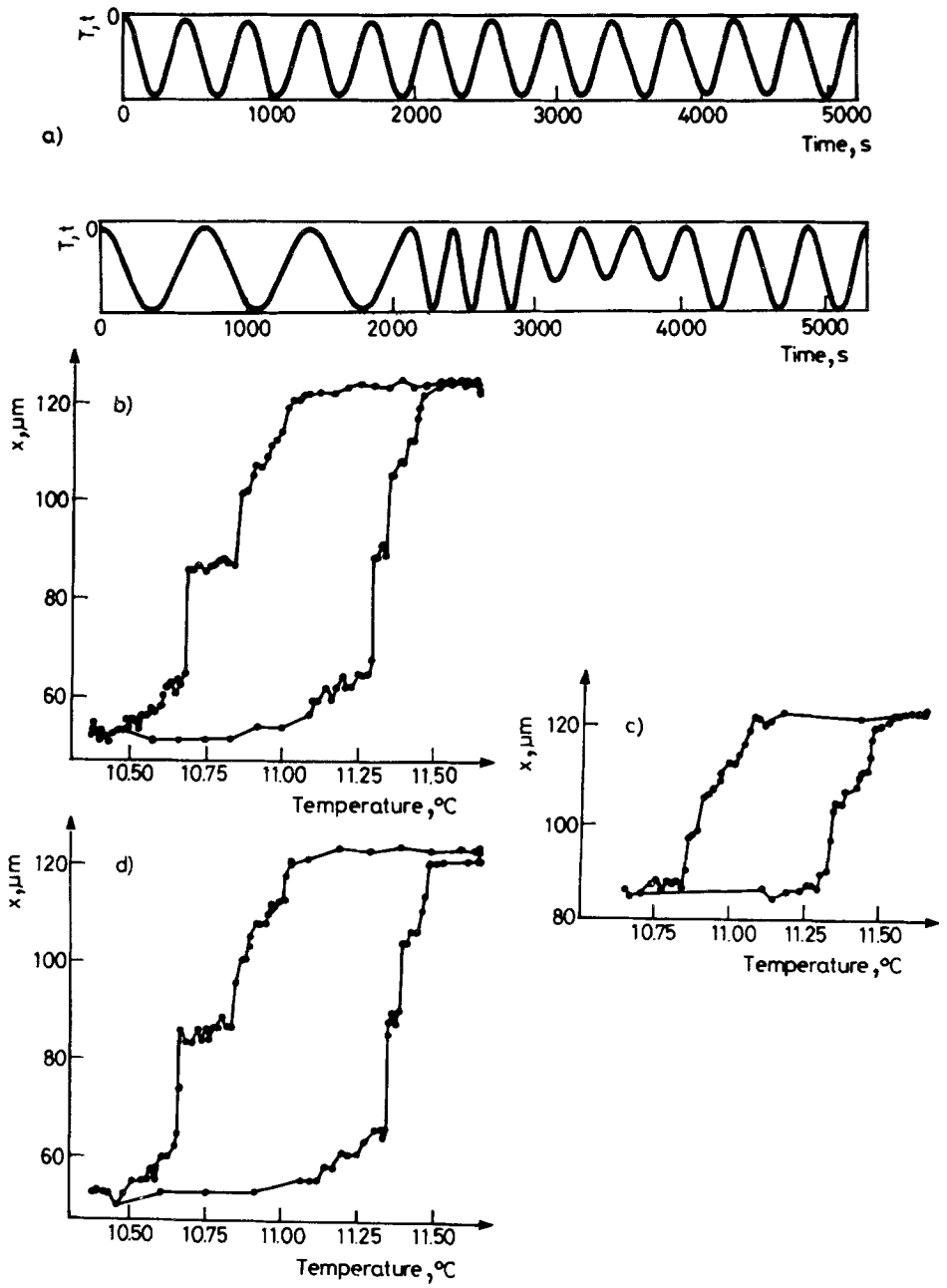

Fig. 20 Temperature programming *vs.* time - Continuous cycling with three different periods a) The "mean" temperatures rates are 14.66, 8.55 and 5.13 mK/s and the amplitudes near 1.25 and 1.00 K
Hysteresis cycle (interface position) *vs.* temperature b) Cycle with the medium temperature rate; c) Cycle with low temperature span; d) Cycle with low temperature rate

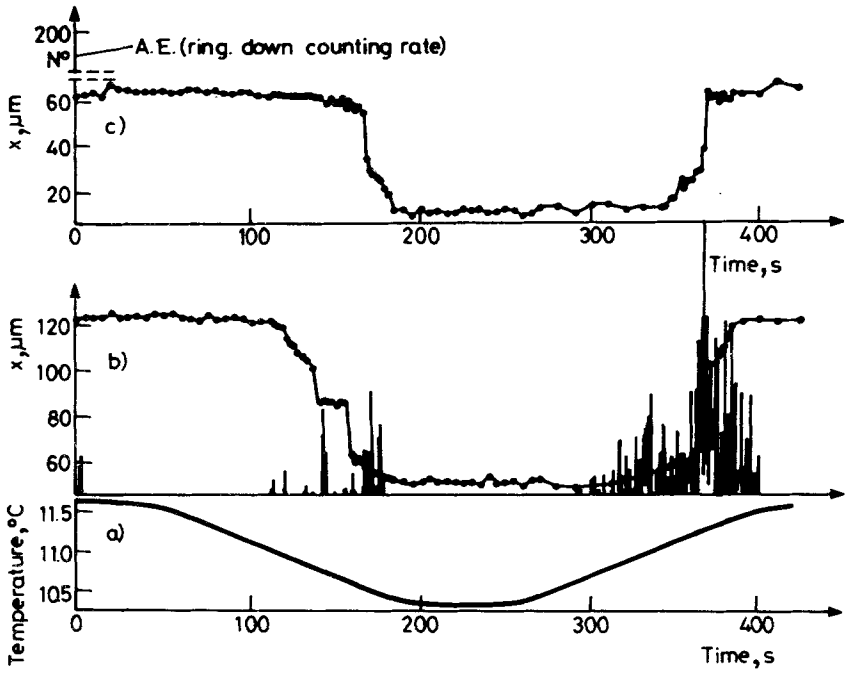

Fig. 21 Acoustic emission and sudden interface movements; a) Temperature *vs.* time, programming with the medium temperature rate ; b) Interface position *vs.* time (β to martensite to β) and all related bursts of AE; c) Other interface position *vs.* time in the same sample

dependent and very sensitive to the surface state. Observations in these domain produces new insights in calorimetric measurements. See in Fig. 18 calorimetric detarminations related to a displacement of 400 μm of single β-m stress free interface. In this case, according to the 1st and 2nd thermodynamic laws, $\int dH \approx 0$.

Acoustic emission: reversibility and stochasticity

Sometimes, the acoustic emission (AE) is assumed to be stochastic, with a counting rate proportional to the rate of the transformation in the material; but the recent results shows:

1) a one-to-one correspondence exists between martensite plate jumps and AE events. Consequently, AE is reproductible as the growth behaviour of the martensite plates.

2) identical thermal cycles preserve the AE pattern and a complete microstructural reversibility seems to exist.

3) cycles whose limiting temperature and rates are modified from cycle to cycle produce instabilities and changes in the growth behaviour.

In Figs 19, A and B thermal cycling has been repeatedly performed between 37.02 and 41.12 C. Two thermal perturbations were introduced within the cycling (2.8 and 5.4°) thus delimiting three zones labelled 1, 2 and 3. The overall amplification of the AE was 50 dB in zone 1, either 50 or 60 dB in zone 2 and 60 dB in zone 3.

Optical observations simultaneous with the detection of acoustic emission during stress-free growing and shrinking of martensitic plates were done. Thermal cycling was made in restrictive conditions (in a reduced temperature interval and with temperature gradients accurately controlled)(Fig. 20). Observations show the existence of an intrinsic hysteresis (near 0.5 K) and one inclined cycle (slope $dx/dt = 100\ \mu m/K$, section near 0.5 mm^2). Evolution with cycling is observed specially in AE measurements (see Fig. 19). The results show the relationship between the appearence, growth, shrinking and motion of martensite plates with the acoustic signals monitored (Fig. 21) and is also able to give a "quantification" of the transformation recoverability in consecutive thermal cycling.

Remarks and conclusions

Different features for thermomechanical treatments TT1, TT2, annealing, polishing and others can be associated with states (atomic order, defects-type and concentration) of the material:

1) the higher concentration of defects created and frozen by water-quenching (TT2) favours the start of the microtransformations at higher temperatures.

2) if one assumes that Ms is the temperature at which the bulk transformation starts, it can be stated that Ms(TT1) > Ms(TT2). This effect can be explained by the different mean-order (B2)-parameter-value. The higher quenching rate in TT2 induces a lower mean-order.

3) the higher amount of defects present in the sample after TT2 produces more internal work, increasing the hysteresis width. Also, creating more and more plates prevents the transformation progress by an increasing of the temperature extension. Optical observations show a big number of martensite plates after TT2 with an important interaction between them. The large elastic interactions between interfaces in this case TT2 play a very important role to this enlargement of the temperature extension.

4) reduction of the surface relief increases the explosivity of the start of the transformation in the first cycle. That is, the fraction of non-thermoelastic transformed material increases; so a more important part of the sample transforms with a great irreversibility (non thermoelastic process). Excess in driving force produces high speed burst-like interphase movements and creates the new defects. The initial growth appears on the sample corners.

5) an easier nucleation (initial growth) at a higher Ms is observed when a worse surface state can be associated with defects generated by mechanical polishing. This defects will be nucleation sites when they had a favourable orientation relative to the surface. Irregular surface characteristics favour that a large quantity of defects could have this favourable orientation.

6) if a sequence of thermal treatments followed by thermal cycling is performed on the same sample (namely TT1-TT2-TT1,...), different behaviours can be observed for each sequence but some characteristics of the previous thermal treatments remain in the sample.

7) if the surface relief is removed by electrolytical polishing, the first forward transformation after TT1 starts in a very explosive way. This non thermoelastic transformation, related to high speed interface movements, generates a large number of defects. The explosive character of the initial part of the first cycle is lost in the second one. This feature makes the area closed by the hysteresis cycle to be higher for the first cycle than for the second one. Also, a high entropy production is observed in the first cycle.

8) the shift of Ms in the second cycle, when remaining constant the others transformation temperatures, reveals that a particular effect in the first cycle exists. This behaviour is related to a delay of the "first nucleation" in the air-quenched samples. It has been pointed out that this temperature delay can be related to absence of defects able to favour the nucleation (first step of the macroscopic growth) in the first cycle. During the first transformation cycle, new defects are created which favour the nucleation in the second cycle. Optical microscopic observations show that the transformation starts at different places in the sample in the first and following cycles, always starting at the sample edges.

9) the enlargement of the hysteresis cycle is related to an increase of the frictional terms. Defects created by the thermal cycling (mostly clusters of dislocations) are responsible of this frictional work. A different shift in $\beta \rightarrow M$ and $M \rightarrow \beta$ indicates that different frictional mechanisms exist in both cases.

10) the strongly discontinous character of the $\beta \leftrightarrow \gamma'$ transformation contributes to the enhancement of the hysteresis width. Annealing acts in two ways: on one hand, by ordering processes, it increases the transforma-

tion temperatures. On the other hand, it decreases the quenched-in defects concentration marking the γ' growth smoother. As a consequence, both the slope increases and the hysteresis width diminishes.

11) the surface orientation plays a definitive role in the transformation dynamics. Different transformation dynamics were obtained for each cut orientation. The discontinuous, burst type, progress of single-variant transformation in samples cut parallel to the habit plane shows the important role that defects play on the transformation dynamics. The hysteresis width can be (partially) associated with this defects. A higher AE detected in this case compared with that of samples non-parallel to the habit plane can be associated, as we will see, at this defects acting as pinnings centers.

12) it is possible to obtain reproducible transformations by cycling when the sample is under stress if the temperature control is better than 0.01 K. Small changes in the temperature domain produce relevant changes in the acoustic activity (temperature distribution and intensity of the acoustic signals). That means that uncontrolled temperature cycling makes the transformation paths to be not reproducible, so the sample does not recover its initial state after each cycle (stochastic character). Observations seems to indicate a link between hysteresis cycle in the surface and the bulk martensite.

13) observations show that the AE is directly related to the sudden release of the energy after the interface overcomes a finite energy barrier which opposes to its motion. These energy barriers can be due to the existence of defects in the sample or the appearance, disappearance or changes of other martensite variants.

14) the plot of the interface position vs. temperature gives an alternative and local representation of the hysteresis loop. The interface movement can stop and then suddenly continue being then detected as AE signal. In fact, the interface motion stop is a cause for the hysteresis width to increase the AE intensity, as well as the hysteresis width, are indicative of the instability due to potential barrier that has to be overcomed. Besides this contribution, the hysteresis loop has an intrinsic character which, at low rates, is temperature and temperature - rate independent. Furthermore, shows a finite slope or intrinsic thermoelasticity connected with the dislocations concentration (about 100 μm/K) which points out that a continuous thermodynamical driving force has to be provided in order to move the interface. This can be related with stacking faults created by the interaction between the moving interface and dislocations.

15) Calorimetric repetitive studises in local transformations show in increased reproducibility, metastable energetic measurements.

* * *

This work has been done in the framework of the cooperation between the Université; de Provence and the Universitat de les Illes Balears. The authors acknowledge the financial support from the inter-universities cooperation program of the DGCYT and SGCI (MEC, Spain).

The authors are also indebted to the working group in Materials Science (A. Amengual, C. Picornell, C. Segui, Palma de Mallorca) for its aid in preparing the manuscript and for the new experimental results presented in this paper.

Some results are obtained in the research cooperation in shape-memory alloys with:

F. C. Lovey, R. Rapacioli and M. Ahlers, Centro Atomico de Bariloche 8400 San Carlos de Bariloche (Argentina)

L. Delaey and J. Van Humbeeck, Katholieke Universiteit Leuven B-3030 Leuven (Heverlee)

J. M. Guilemany, Universitat de Barcelona E-08028 Barcelona

or in the research cooperation in calorimetry and signal processing with:

W. Zielenkiewicz, Instytut Chemii Fizycnej, Polska Akademia Nauk 01-224 Warszawa (Poland)

J. L. Macqueron, Institut National des Sciences Appliqu;es F-69621 Villeurbanne CEDEX

M. Rodriguez de Rivera, Universidad Politecnica de Canarias E-35017 Tafira Baja, Gran Canaria

The present Work has been financially supported by CICYT (PA 86-0079 and MAT 89-0407-C03).

V. T. gives thanks to the University of provence for their financial support.

References

1 E. Calvet, Microcalorim;trie, Masson Ed., Paris, 1956.

J. Navarro and V. Torra, Proc. II Krajowa Konferencja Kalorymetrii i Analizy Termicznej, Zakopane 11-19/09/1976, Instytut Chemii Fizicnej, Polska Akademia Nauk Ed., Warsaw

P. Ch. Gravelle, Catal. Re. Sci. Eng., 16 (1977) 37.

E. Cesari, J. Navarro, V. Torra, P. Ch. Gravelle, J. L. Petit, R. Point, J. Gutenbaum, J. Hatt, E. Utzig and W. Zielenkiewicz, J. Therm. Anal., 20 (1981) 47.

E. Cesari, J. Navarro, V. Torra, J. L. Macqueron, R. Prost, J. P. Dubes and H. Tachoire, Bull. Soc. Chim. Fr., I (1982) 49.

E. Cesari, J. Navarro, V. Torra, J. L. Macqueron, R. Prost, J. P. Dubes and H. Tachoire, Bull. Soc. Chim. Fr., I (1982) 54.

E. Cesari, A. Planes, V. Torra, J. L. Macqueron, J. P. Dubes, R. Kechavarz and H. Tachoire, Bull. Soc. Chim. Fr., I (1983) 89.

H. Tachoire, J. L. Macqueron and V. Torra, Thermochemistry and Its Applications to Chemical and Biochemical Systems, M. A. V. Ribeiro da Silva Ed., NATO ASI Series, 119 (1984) 77.

H. Tachoire, J. L. Macqueron and V. Torra, Thermochim. Acta, 105 (1986) 333.

2 See, for example, the Proceedings of the International Conferences on Martensitic Transformations (ICOMAT) Proc. ICOMAT 82, J. Phys., C4 (1982)
Proc. ICOMAT 86, The Japan Institute of Metals (1987)
International Summer Course on Martensitic Transformations, ICOMAT 82, Dept. Metaalkunde en T. M., Katholieke Universiteit Leuven Ed., (1982)
Annual Reports of Dept. Metaalkunde en T. M., Katholieke Universiteit Leuven
3 C. Picornell, C. Segui, V. Torra, J. Hernaez and C. Lopez del Castillo, Thermochim. Acta, 91 (1985) 311.
C. Picornell, C. Segui, V. Torra, C. Auguet, Ll. Mañosa, E. Cesari and R. Rapacioli, Thermochim. Acta, 106 (1986) 209.
J. Van Humbeeck, D. Van Hulle, L. Delaey, J. Ortin, C. Segui and V. Torra, Trans. Jap. Inst. Met., 28 (1987) 383.
R. Rapacioli, V. Torra, E. Cesari, J. M. Guilemany and J. R. Miguel, Scripta Metall., 22 (1988) 261.
C. Picornell, C. Segui, V. Torra and R. Rapacioli, Scripta Metall., 22 (1988) 999.
A. Amengual, C. Picornell, R. Rapacioli, C. Segui and V. Torra, Thermochim. Acta, 145 (1989) 101.
4 Ll. Mañosa, C. Picornell, C. Segui and V. Torra, J. Acoust. Emiss., 5 (1986) 549.
F. C. Lovey, C. Picornell, R. Rapacioli, C. Segui and V. Torra, Thermochim. Acta, 113 (1987) 171.
A. Amengual, F. Marco, Ll. Mañosa, C. Picornell, C. Segui and V. Torra, Thermochim. Acta, 116 (1987) 195.
F. C. Lovey, V. Torra, J. M. Guilemany and E. Cesari, Mater. Lett., 5 (1987) 159.
F. C. Lovey, J. Ortin and V. Torra, Phys. Lett., A121 (1987) 352.
A. Amengual, F. Garcias, F. Marco, C. Segui and V. Torra, Acta metall., 36 (1988) 2329.
F. C. Lovey, A. Amengual, V. Torra and M. Ahlers, Phil. Mag. A, 61 (1990) 159.
B. G. Mellor, J. M. Guilemany, J. R. Miguel, J. Fernandez, A. Amengual, F. C. Lovey and V. Torra, Scripta Metall., 24 (1990) 241.
5 V. Torra, J. M. Guilemany and E. Cesari, Thermochim. Acta, 99 (1986) 19.
J. Ortin, H. Tachoire and V. Torra, Thermochim. Acta, 121 (1987) 333.
H. Tachoire and V. Torra, Can. J. Chem., 67 (1989) 983.
A. Amangual and V. Torra, J. Phys. E: Sci. Instr., 22 (1989) 433.
V. Torra and H. Tachoire, Trait. Therm. (Fr.), 234 (1990) 35.
6 W. Zielenkiewicz and E. Margas, Bull. Acad. Polon. Sci., Ser. Sci. Chim., 16 (1968) 101 and 16 (1968) 133.
E. Margas, Bull. Acad. Polon. Sci., Ser. Sci. Chim., 17 (1969) 557.
V. Torra, E. Rojas and M. Zamora, An. Fis., 67 (1971) 119.
E. Margas, A. Tabaka and W. Zielenkiewicz, Bull. Acad. Polon. Sci., Ser. Sci. Chim., 20 (1972) 323.
W. Zielenkiewicz and E. Margas, Bull. Acad. Polon, Sci., Ser. Sci. Chim., 21 (1973) and 21 (1973) 251.
K. L. Churney, E. D. West and G. T. Armstrong, NBSIR (1973) 73.
J. L. Macqueron, J. Navarro and V. Torra, An. Fis., 73 (1977) 163.
E. Margas and W. Zielenkiewicz, Bull. Acad. Polon. Sci., Ser. Sci. Chim., 26 (1978) 503.
E. Cesari, J. Hatt, E. Margas, J. Navarro, V. Torra, E. Utzig and W. Zielenkiewicz, Bull. Acad. Polon. Sci., Ser. Sci. Chim., 28 (1980) 297.
J. Navarro, E. Cesari, V. Torra, J. L. Macqueron, J. P. Dubes and H. Tachoire, Thermochim. Acta, 52 (1982) 175.
E. Cesari, J. Ortin, J. Viñals, J. Hatt, W. Zielenkiewicz and V. Torra, Thermochim. Acta, 71 (1983) 351.
7 E. Rojas, V. Torra and M. Zamora, An. Fis., 67 (1971) 359.
J. Navarro, V. Torra and E. Rojas, An. Fis., 67 (1971) 367.
H, Navarro, E. Rojas and V. Torra, Rev. Gen. Therm. Fr., 12 (1973) 1137.
E. Cesari, V. Torra, J. Navarro, E. Utzig and W. Zielenkiewicz, Bull. Acad. Polon. Sci., Ser. Sci. Chim., 26 (1978) 731.
E. Cesari, J. Navarro, J. L. Macqueron and V. Torra, Thermochim. Acta, 39 (1980) 73.
E. Cesari, J. Ortin, P. Pascual, V. Torra, J. Viñals, J. L. Macqueron, J. P. Dubes and H. Tachoire, Thermochim. Acta, 48 (1981) 367.

E. Cesari, J. Ortin, V. Torra, J. Vinals, J. L. Macqueron, J. P. Dubes and H. Tachoire, Thermochim. Acta, 53 (1982) 29.
J. Rodriguez, C. Rey, V. Perez-Villar, V. Torra, J. Ortin and J. Viñals, Thermochim. Acta, 63 (1983) 331.
J. L. Macqueron, J. Ortin, G. Thomas and V. Torra, Thermochim. Acta, 67 (1983) 213.
J. Ortin, V. Torra, T. Castan and E. Cesari, Thermochim. Acta, 70 (1983) 123.
J. Rodriguez, C. Rey, V. Perez-Villar, V. Torra, J. Ortin and J. Vinals, Thermochim. Acta, 75 (1984) 51.
J. Rodriguez, C. Rey, V. Perez-Villar, J. P. Dubes, H. Tachoire and V. Torra, Thermochim. Acta, 76 (1984) 325.
F. Marco, M. Rodriguez de Rivera, J. Ortin and V. Torra, Thermochim. Acta 89 (1985) 315.
E. Margas, J. Hatt, W. Zielenkiewicz and V. Torra, Sci. Instrum., 2 (1987) 55.

Zusammenfassung – Es werden kalorimetrische und thermoanalitische Verzuchsanordnungen zur Untersuchung von martenzitischen Umwandlungen bei Form-Gedächtnis-Legierungen beschrieben. Es wurde folgendes ermittelt: Umwandlungstemperatur, Enthalphie- und Entropieänderungen und die Dynamik der Erscheinung. Es werden die Hystereseschleife als auch die makroskopischen Erscheinung der Umwandlung gegeben.

Mittels des verbesserten hochauflösenden Thermoanalyseverfahrens wurden lokale Untersuchungen durch - und neue Erscheinungen wie eigen Thermoelasticität, Zeitskalen usw. eingeführt.